

# Testing machine learning algorithms for the prediction of depositional fluxes of the radionuclides ${}^7\text{Be}$ , ${}^{210}\text{Pb}$ and ${}^{40}\text{K}$ .

Pedro De la Torre Luque<sup>1</sup>, Concepcion Duenas<sup>2</sup>, Elisa Gordo<sup>3</sup>, and Sergio Cañete<sup>3</sup>

<sup>1</sup>Istituto Nazionale di Fisica Nucleare Sezione Bari

<sup>2</sup>University of Malaga

<sup>3</sup>University of Málaga

November 23, 2022

## Abstract

The monthly depositional fluxes of three natural radionuclides ( ${}^7\text{Be}$ ,  ${}^{210}\text{Pb}$  and  ${}^{40}\text{K}$ ) were measured at a Mediterranean coastal station (Malaga, Southern Spain) over a 14-year period from 2005 to 2018, corresponding to 168 monthly samples. The study of these radionuclides provides valuable information on the atmospheric air circulation, transportation and erosion processes as well as a control of the environmental radioactivity. In this work, the depositional fluxes of these radionuclides are investigated and their relations with several atmospheric variables, such as air temperature, pressure or precipitations, have been studied by applying two popular machine learning methods: Random Forest and Neural Network algorithms. We extensively test different configurations of these algorithms and demonstrate their predictive ability for reproducing depositional fluxes of  ${}^7\text{Be}$ ,  ${}^{210}\text{Pb}$  and  ${}^{40}\text{K}$ . We use the Pearson-R correlation coefficient and the mean average error to evaluate the predictions of the developed models, revealing that the models derived with Neural Networks achieve slightly better results, in average, although similar, having into account the uncertainties. The mean Pearson-R coefficients, evaluated with a k-fold cross-validation method, are around 0.85 for the three radionuclides using Neural Network models, while they go down to 0.83, 0.79 and 0.8 for  ${}^7\text{Be}$ ,  ${}^{210}\text{Pb}$  and  ${}^{40}\text{K}$ , respectively, for the Random Forest models. Additionally, applying the Recursive Feature Elimination technique we determine the variables more correlated with the depositional fluxes of these radionuclides, which elucidates the main dependencies of their temporal variability.

1 **Testing machine learning algorithms for the prediction**  
2 **of depositional fluxes of the radionuclides  $^7\text{Be}$ ,  $^{210}\text{Pb}$**   
3 **and  $^{40}\text{K}$ .**

4 **P. De La Torre Luque<sup>1</sup>, C. Dueñas<sup>2</sup>, E. Gordo<sup>3</sup>, S. Cañete<sup>3</sup>**

5 <sup>1</sup>Istituto Nazionale di Fisica Nucleare, Bari, via Orabona 4, I-70126 Bari, Italy

6 <sup>2</sup>Department of Applied Physics I, Faculty of Sciences, University of Malaga, Spain

7 <sup>3</sup>Central Research Services (SCAI), University of Malaga, 29071-Malaga, Spain

8 **Key Points:**

- 9
- 10 • Machine learning methods allow us to improve predictions on environmental ra-  
11 dioactivity.
  - 12 • Correlation found between Solar cycle and depositional fluxes of crustal radionu-  
13 clides  $^{210}\text{Pb}$  and  $^{40}\text{K}$ .
  - 14 • Machine learning models adapted for studying depositional fluxes of  $^7\text{Be}$ ,  $^{210}\text{Pb}$   
and  $^{40}\text{K}$ .

---

Corresponding author: P. De La Torre Luque, [pedro.delatorreluque@fysik.su.se](mailto:pedro.delatorreluque@fysik.su.se)

## Abstract

The monthly depositional fluxes of three natural radionuclides ( $^7\text{Be}$ ,  $^{210}\text{Pb}$  and  $^{40}\text{K}$ ) were measured at a Mediterranean coastal station (Malaga, Southern Spain) over a 14-year period from 2005 to 2018, corresponding to 168 monthly samples. The study of these radionuclides provides valuable information on the atmospheric air circulation, transportation and erosion processes as well as a control of the environmental radioactivity. In this work, the depositional fluxes of these radionuclides are investigated and their relations with several atmospheric variables, such as air temperature, pressure or precipitations, have been studied by applying two popular machine learning methods: Random Forest and Neural Network algorithms. We extensively test different configurations of these algorithms and demonstrate their predictive ability for reproducing depositional fluxes of  $^7\text{Be}$ ,  $^{210}\text{Pb}$  and  $^{40}\text{K}$ . We use the Pearson-R correlation coefficient and the mean average error to evaluate the predictions of the developed models, revealing that the models derived with Neural Networks achieve slightly better results, in average, although similar, having into account the uncertainties. The mean Pearson-R coefficients, evaluated with a k-fold cross-validation method, are around 0.85 for the three radionuclides using Neural Network models, while they go down to 0.83, 0.79 and 0.8 for  $^7\text{Be}$ ,  $^{210}\text{Pb}$  and  $^{40}\text{K}$ , respectively, for the Random Forest models. Additionally, applying the Recursive Feature Elimination technique we determine the variables more correlated with the depositional fluxes of these radionuclides, which elucidates the main dependencies of their temporal variability.

## 1 Introduction

The use of natural radionuclides as markers for studying the atmospheric circulation provides valuable information about the complex mechanisms involved. It is common to employ different natural radionuclides as tracers and chronometers in aquatic and atmospheric systems (Wogman et al., 1968; Martell, 1970; Schuler et al., 1991) and they have demonstrated to be very useful in studies dedicated to understand the mechanisms and rates of removal of aerosols (Baskaran et al., 1993). In this work, we aim at the study of a predictive model for the depositions of fallout radionuclides  $^7\text{Be}$ ,  $^{210}\text{Pb}$ , and  $^{40}\text{K}$ , whose different origins allow us to infer important features of the atmospheric circulation, erosion processes, transportation and deposition of soils and sediments from episodic to long-term timescales.

$^7\text{Be}$  is a cosmogenic radionuclide originated by spallation reactions of cosmic rays with light atmospheric nuclei, such as nitrogen and oxygen (Lal et al., 1958) that has a decay half-life of  $T_{1/2} = 53$  day. Thus, this nuclide is mostly produced in the stratosphere and reach the troposphere in periods of air exchange between these two layers. This is why the production of  $^7\text{Be}$  is dependent on altitude, latitude and solar cycle but has negligible dependence on longitude (Baskaran et al., 1993; Dueñas et al., 2017).

In contrast,  $^{210}\text{Pb}$ , with a decay half-life of  $T_{1/2} = 22.3$  yr, is produced from the radioactive decay of  $^{222}\text{Rn}$ , the only gaseous decay product of  $^{238}\text{U}$  series. Therefore,  $^{210}\text{Pb}$  is found in larger concentrations near the ground and with important dependence on the distribution of land and seas (Moore et al., 1973; Wilkening et al., 1975; Preiss et al., 1996; Garcia-Orellana et al., 2006)

The atmospheric  $^{40}\text{K}$  ( $T_{1/2} = 1.3 \cdot 10^9$  yr) is related to a crustal origin, from most kinds of soil, which is usually found in association with other re-suspended materials, as PM10 (particulate matter with diameter  $10 \mu\text{m}$ ) from the African continent (Karlsson et al., 2008; Dueñas et al., 2011).

Several works in the past have been dedicated to study the relations between the concentrations or depositional fluxes of these radionuclides with different environmental variables for different latitudes and longitudes. In this work, we employ a large dataset

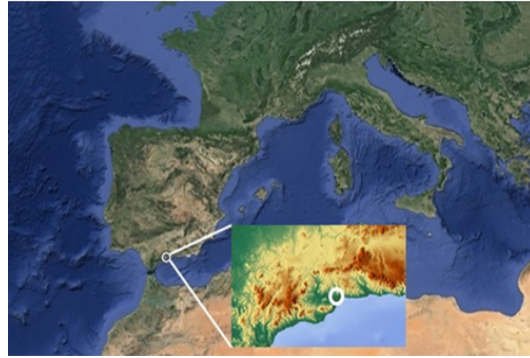


**Figure 1.** Physical map showing the location of the study area. The zoomed window shows the exact position of study area, in Málaga.

(168 monthly measurements, from January 2005 to December 2018) of environmental variables and the fluxes of  $^7\text{Be}$ ,  $^{210}\text{Pb}$ , and  $^{40}\text{K}$  radioactivity in the Mediterranean coastal region of Málaga (Southern Spain). Similar studies were carried out in the same zone in the past and reported some important results, such as correlations with particulate material (PM10 levels) or with other environmental variables included in this work (Dueñas et al., 2004, 2009, 2011, 2017).

Here, we are exploring new methods of studying the complex relations between the depositional flux of these radionuclides and atmospheric variables, using machine learning algorithms. Machine learning (ML) techniques (Carbonell et al., 1983) provide a promising tool in the prediction of any magnitude which depends on a large number of variables and exhibits complex relations with them. Particularly, we are focused here on the implementation of these methods for the prediction of depositional fluxes of the mentioned radionuclides. These models allow us to identify subtle long-term relationships between the temporal variability of the depositional fluxes and other environmental cycles, like the Solar cycle or atmospheric cycles. Additionally, reproducing these fluxes allow us discern the real agents affecting the depositions of these radionuclides and could provide another tracer of anomalous (artificial) radiation episodes. In addition, we argue that these kind of models could be extended to different zones, always that measurements are available, to study relations with other variables not yet taken into account.

## 2 Materials and measurements

### 2.1 Study area

Málaga ( $4^\circ 28' 8''$  W;  $36^\circ 43' 40''$  N), is the major coastal city in the Andalusian region situated in the south-east of Spain (see Figure 1), on the Mediterranean coast and, therefore, has a climate influenced by continental and maritime air masses. The predominant winds are easterly (SE) and westerly (NW). The climate is temperate, with contrasting wet (approximately October–April) and dry (approximately May–September) periods (Dueñas et al., 2012). The city is almost surrounded by mountains, which cause a special wind regime. Due to its geographical proximity to the African continent, our study area is frequently affected by intrusions of air masses with high concentrations of atmospheric particulate matter (Escudero et al., 2005). The sampling point is located on the flat roof of the Central Research Services (SCAI) building at the University of Málaga, at a height of 10 m above the ground and approximately at 5 km from the coastline, near the airport and surrounded by roads with traffic exhaust.

98

## 2.2 Data extraction

99

100 Bulk deposition samples were collected from January 2005 to December 2018. Sam-  
 101 ples were collected monthly using a collector that it is slightly tilted stainless steel tray  
 102 1 m<sup>2</sup> in area and a polyethylene vessel of 60 L capacity for rainwater sample reservoir.  
 103 A volume of 6 L of the bulk deposition (the sum of wet deposition flux and the gravi-  
 104 tational sedimentation fraction of the dry deposition) was reduced via evaporation to ap-  
 105 proximately 1 L and transferred to a Marinelli geometry container for gamma counting.  
 106 The method and processing procedures were described previously (Dueñas et al., 2011).  
 The atmospheric fluxes were calculated using the expression:

$$F = A/St \text{ (Bq m}^{-2} \text{ month}^{-1}\text{)}, \quad (1)$$

107

108 where  $A$  is the activity in the sample obtained from the gamma spectra,  $S$  is the sur-  
 109 face area of the collector and  $t$  is the duration of sampling time. Additionally, aerosol  
 110 samples were collected weekly in cellulose filters of 0.8  $\mu\text{m}$  pore size and 47 mm diam-  
 111 eter with an air sampler (Radeco, mod AVS-28A) at a flow rate of 40 l/min. A monthly  
 112 composite sample containing 4 or 5 filters (depending on the number of weeks each month)  
 was formed for the gamma analysis.

113

114 Radiometric measurements were performed by low-level gamma spectrometry with  
 115 a coaxial-type germanium detector (Canberra Industries Inc., USA), with a relative ef-  
 116 ficiency of 20% and it was calibrated using certified reference gamma ray cocktail. Each  
 117 sample was measured for 172,000 s. Gamma spectra analyses were performed with the  
 118 Genie2K spectrometry software version 2.0 (Canberra Industries Inc., USA). The char-  
 119 acteristic gamma peaks selected for the determination of the different radionuclides were:  
 120 477.6 keV for <sup>7</sup>Be, 1460.81 keV for <sup>40</sup>K and 46.5 keV for <sup>210</sup>Pb. To validate the meth-  
 121 ods, our lab routinely participates in interlaboratory comparisons to measure gamma-  
 122 emitting radionuclides, in different types of samples, organized by the International Atomic  
 123 Energy Agency (IAEA), the Joint Research Centre (JRC), and the Spanish Nuclear Safety  
 124 Council (CSN). Further details of the low-background gamma-ray detection system have  
 been previously described by refs. Dueñas et al. (1999, 2004).

125

126 The meteorological data (temperature, relative humidity, distance travelled monthly  
 127 by the wind and precipitation) used in this study were obtained from the nearest sta-  
 128 tion network of the Spanish Meteorological Agency (AEMET) (500 m away from the sam-  
 129 pling site). Days affected by African dust outbreaks have been obtained from CALIMA  
 130 project ([www.calima.es](http://www.calima.es)). The monthly sunspots number were obtained from NOAA's  
 Space Weather Prediction Center (SWPC).

131

132 Additionally, data of daily concentrations of particulate matter fraction PM10 were  
 133 obtained from Carranque (36° 43' 40" N; 4° 28' 4" W), a monitoring station belonging  
 134 to the regional Atmospheric Pollution Monitoring network managed by the Environmen-  
 tal Health Service of the Andalusian Government.

135

## 3 Methods: description of the algorithms applied and cross-validation framework

136

137

138 ML techniques have demonstrated their predictive power in a variety of fields, from  
 139 medicine (e.g. (Lapedes et al., 1988)) to astrophysics (e.g. (Schaefer, C. et al., 2018), (Graff  
 140 et al., 2014)), used for both classification (as in (Williams et al., 2006)) and numerical  
 141 forecasting (see, for example, refs. Sarkar et al. (2009); vStencl and Stastny (2011)). Gen-  
 142 erally, ML methods are used to find the relation between a set of input variables and an  
 143 output variable one is interested in. These variables are usually called features and la-  
 144 bels, respectively. In the present study, the labels are the monthly depositional fluxes  
 145 collected from 2005 to 2018 and the features are the atmospheric variables gathered in  
 146 the same period. Earlier studies have demonstrated that it is possible to find linear re-  
 lations between atmospheric variables and the depositional fluxes of these radionuclides,

147 although the uncertainties related to this determination become too large to have ac-  
 148 curate predictions. Using these methods we aim at obtaining more precise predictions  
 149 on the depositional fluxes that could be used, e.g., to reliably detect the emission of ar-  
 150 tificial radiation or other non-expected radiation sources.

151 The relation between features and labels is progressively adjusted by iterating over  
 152 the amount of data samples given to the algorithm, therefore the larger the amount of  
 153 samples used to feed (or train) the algorithm the better the predictions become. The data  
 154 sample used to adjust the algorithm is called training dataset and this adjustment pro-  
 155 cess is known as the training phase, which basically consists on tuning some training pa-  
 156 rameters in order to predict the correct labels given. The algorithm adjusts itself in each  
 157 iteration by comparing its predicted label with the correct label. Then, in order to evalu-  
 158 ate the performance of the model one must provide it with new input data (i.e. these  
 159 features must be different from the training data to ensure unbiased or over-fitted eval-  
 160 uations of the algorithm effectiveness). In this way, we can “grade” or “score” the model  
 161 performance by comparing the predicted outputs with the real labels in what is called  
 162 the test phase. The new set of data used in this phase is called test data.

163 Two different supervised algorithms have been implemented in this study; Neural  
 164 Networks and Random Forest techniques, and their ability to predict depositional fluxes  
 165 has been extensively tested for different configurations and for the depositional fluxes  
 166 of the  ${}^7\text{Be}$ ,  ${}^{210}\text{Pb}$  and  ${}^{40}\text{K}$  radionuclides. Very few works have been published using ML  
 167 techniques to predict depositional fluxes and none of them systematically analyzing their  
 168 performance. An example of these studies can be found in ref. Chham et al. (2018), but  
 169 a deeper research on the efficiency of these techniques is necessary.

170 The most popular ML algorithm is the *Artificial Neural Network* (ANN) model.  
 171 Neural networks can learn complex patterns using layers of neurons which mathemat-  
 172 ically transform the data. The layers between the input and output are referred to as  
 173 “hidden layers”. A Neural Network can learn relationships between the features that other  
 174 algorithms cannot easily discover, including also complex non-linear relations.

175 Moreover, we used an alternative and less demanding (in terms of resources) tech-  
 176 nique, the *Random Forest* algorithm <sup>1</sup>, which, in turn, is not able to consider non-linear  
 177 features in the relations between the features. This algorithm relies in an ensemble of  
 178 decision trees which are combined to get averaged predictions. Each tree uses a sub-sample  
 179 of the full data set, randomly selected, and progressively divides it into different nodes  
 180 (or leaves) depending on certain quantitative (or qualitative, in case the tree is applied  
 181 for a classification problem) criteria decided by the algorithm.

182 We have divided our collected data set into a training set, containing the 80-85%  
 183 of the full data set, and a test set that allows us to quantify the performance of our pre-  
 184 dictions. The list of features (meteorological or atmospheric variables) employed is based  
 185 on monthly averages (or monthly accumulated) and it consists of: Air temperature (in  
 186 °C), relative humidity level (%) number of days affected by African dust outbreaks (in-  
 187 trusions), distance travelled monthly by the wind (in km), pressure (hPa), sunspot num-  
 188 ber, amount of rainfall ( $\text{dm}^3$ ), PM10 level ( $\mu\text{g}/\text{m}^3$ ), seasonal factor (from 1, for winter,  
 189 to 4, for spring), monthly factor (from 1, for January, to 12, for December), total rain-  
 190 fall duration (min), humid days, dry days and time between rains (in days). For both  
 191 algorithms, the labels (depositional fluxes) are normalized, since this allows a better per-  
 192 formance of the algorithm.

193 A Neural Network in which the input features first result into 8 units (1st hidden  
 194 layer) and then into 4 units (second hidden layer) have been found to be the most ad-  
 195 equate, as it is depicted in the Appendix A. The implementation of the Neural Network

---

<sup>1</sup>Specifically the method *RandomForestRegressor* given by the package of *sklearn.ensemble*

	<sup>7</sup> Be	<sup>210</sup> Pb	<sup>40</sup> K
Learning rate	2.1e-3	2.1e-3	2.2e-3
Decay rate	5.e-6	5.e-5	2.4e-6

**Table 1.** Main hyperparameters (i.e. the values needed to control the learning process in ML algorithms) used in the Adam optimizer, adjusted for each of the radionuclides studied.

196 has been achieved by using the *Python Keras* (Chollet, 2015) library. The connections  
 197 between the input features and the first hidden layer, as well as between the first and  
 198 second hidden layers use the Rectified Linear Unit (ReLU) as activation function and  
 199 the connections from the second hidden layer and the output units are calculated with  
 200 a linear activation function.

201 The model performance was optimized including a step of batch normalization and  
 202 dropout (finding the best results adjusting it to the 10% of the sample) after each of the  
 203 hidden layers. In addition, the adaptive moment estimation optimizer, or *Adam* opti-  
 204 mizer<sup>2</sup>, was found to get the best performance for every one of the radionuclides. On top  
 205 of this, the best results were found when taking the natural logarithm of the values for  
 206 the features, as expected, and setting the mean absolute error metrics as the loss func-  
 207 tion.

208 Different configurations of the neural networks models and the hyperparameters  
 209 involved (i.e. the values needed to control the learning process in ML algorithms) were  
 210 refined by applying a simple random search method (i.e. probing different hyperparam-  
 211 eters in an equally spaced grid of values) (Bergstra & Bengio, 2012). The optimization  
 212 of the combination of these hyperparameters is left for a next work. In table 3, we show  
 213 the main hyperparameters tuned for the *Adam* optimizer for each radionuclide. The rest  
 214 of hyperparameters needed by the optimizer were set to their default values given by the  
 215 *keras* method.

216 For the Random Forest algorithm, it was found that using the features values nor-  
 217 malized, instead of their natural logarithm, gave better results. Then, the main hyper-  
 218 parameters were adjusted for each of the nuclides, setting the mean absolute error (MAE)  
 219 as criterion for splitting the nodes and a minimum number of samples required to split  
 220 an internal node (*min\_samples\_split*) to 3. The number of decision trees (also known as  
 221 number of estimators) used in the model was set to be 680 for <sup>7</sup>Be and <sup>210</sup>Pb and 280  
 222 for <sup>40</sup>K.

223 The results from both algorithms and for the three radionuclides are shown and  
 224 compared in the next section, in which we fully demonstrate their ability for reproduc-  
 225 ing the data and systematically explore the statistical errors around these predictions  
 226 as well as the main features involved.

## 227 4 Results: predictive power of the algorithms

228 As a first step before running our models, we randomly shuffle the features and la-  
 229 bels and, then, they are divided into a training and a test sets. Once the model is trained,  
 230 we rate its performance by comparing the predictions with the test labels, correspond-  
 231 ing to a 15-20% of the full data sample, using the mean percentage error and the Pearson-

<sup>2</sup> <https://keras.io/api/optimizers/>

232 R index value. While the former is an indicator of the quantitative differences between  
 233 test labels and predictions, the latter is a good indicator of the trend similarities between  
 234 the two sets.

235 In order to compare these results with a reference model, we applied the same kind  
 236 of evaluation as applied for the ML algorithms to the model found in the linear regres-  
 237 sion analysis presented in ref. Dueñas et al. (2017) for the  $^7\text{Be}$  radionuclide. This anal-  
 238 ysis yields a linear relation between the depositional flux of  $^7\text{Be}$  and the amount of rain-  
 239 fall (the variable which shows the largest correlation with the depositional flux of every  
 240 radionuclide) of:

$$Flux_{Be} = 6.33 + 2.6 \times \text{rainfall} \quad (2)$$

241 Then, the evaluation is carried out by using a portion of 25 randomly selected mea-  
 242 surements (similar to the amount of samples in the test sets used for the ML algorithms  
 243 applied) of  $^7\text{Be}$  and amount of rainfall (corresponding to the same date) and measured  
 244 the Pearson-R index and mean error of the predictions obtained with this reference model.  
 245 In order to have a robust idea on the value of these metrics, we repeated this for 100 times  
 246 (analogous to what is done in section 4.1), with different randomly selected samples of  
 247 25 measurements, and computed the average value. These metrics result in a mean R  
 248 index of  $\sim 0.45 \pm 0.4$  and a maximum R index of 0.95, while the mean percentage er-  
 249 rors were of  $103 \pm 150\%$ . Having these reference metric values is necessary to compare  
 250 to the quantitative results of the Random Forest and Neural Network algorithms stud-  
 251 ied here. In Figure B1 (Appendix B), we display the comparison between the predictions  
 252 from the reference model and the depositional flux measurements for one of these sam-  
 253 ples.

254 In comparison, in Figure 2, we show some of the best results acquired from the Neu-  
 255 ral Network and Random Forest algorithms for all the studied radionuclides, which demon-  
 256 strates that these algorithms can allow us to significantly improve our predictions on de-  
 257 positional fluxes with respect to traditional methods. Here, we highlight that these are  
 258 predictions obtained from their corresponding atmospheric variables, and remark the im-  
 259 portance of evaluating these predictions with data not used for the training phase, since  
 260 this highly biases our evaluation. As we can see by the Pearson-R value, these predic-  
 261 tions are able to suitably reproduce the labels trend with respect to the atmospheric vari-  
 262 ables. In addition, we find mean absolute errors of the order 50% usually, which are well  
 263 below the error levels found using linear regressions (as shown above) and are similar to  
 264 the experimental uncertainties in the determination of these fluxes, which can be  $\mathcal{O}(10\%)$ ,  
 265 as shown in refs. Herranz et al. (2008); Heydorn (2004). In this case, it has been observed  
 266 that high-flux values are difficult to be matched, which may be related to periods of anoma-  
 267 lous radiation doses. Nevertheless, this requires a dedicated study of those points and  
 268 their temporal behaviour, which is beyond the scope of this paper. Further sources of  
 269 uncertainty in these comparisons mainly come from the statistical uncertainties related  
 270 to the measurement of the atmospheric variables and variables not included in the model.

271 Surprisingly, the models make good predictions also for the  $^{40}\text{K}$  nuclide, even with  
 272 a considerably smaller number of samples available for it. On top of this, we found that  
 273 the absolute percentage errors follow a similar distribution for each radionuclide and both  
 274 algorithms. They are well described with a Gamma probability distribution, which ex-  
 275 hibits a slightly negative mode and a slightly positive median. This is likely due to the  
 276 fact that the distribution of depositional fluxes is also be very well reproduced with a  
 277 Gamma function. A representative example of these distributions for the Neural Net-  
 278 work and Random Forest algorithms is shown in Figure 3 for the  $^7\text{Be}$  radionuclide af-  
 279 ter gathering several repetitions for different test sets used. The fact that these errors  
 280 follow such distribution can be used to statistically diagnose anomalous episodes of ra-  
 281 diation doses. We noticed that the Random Forest models produce slightly larger me-

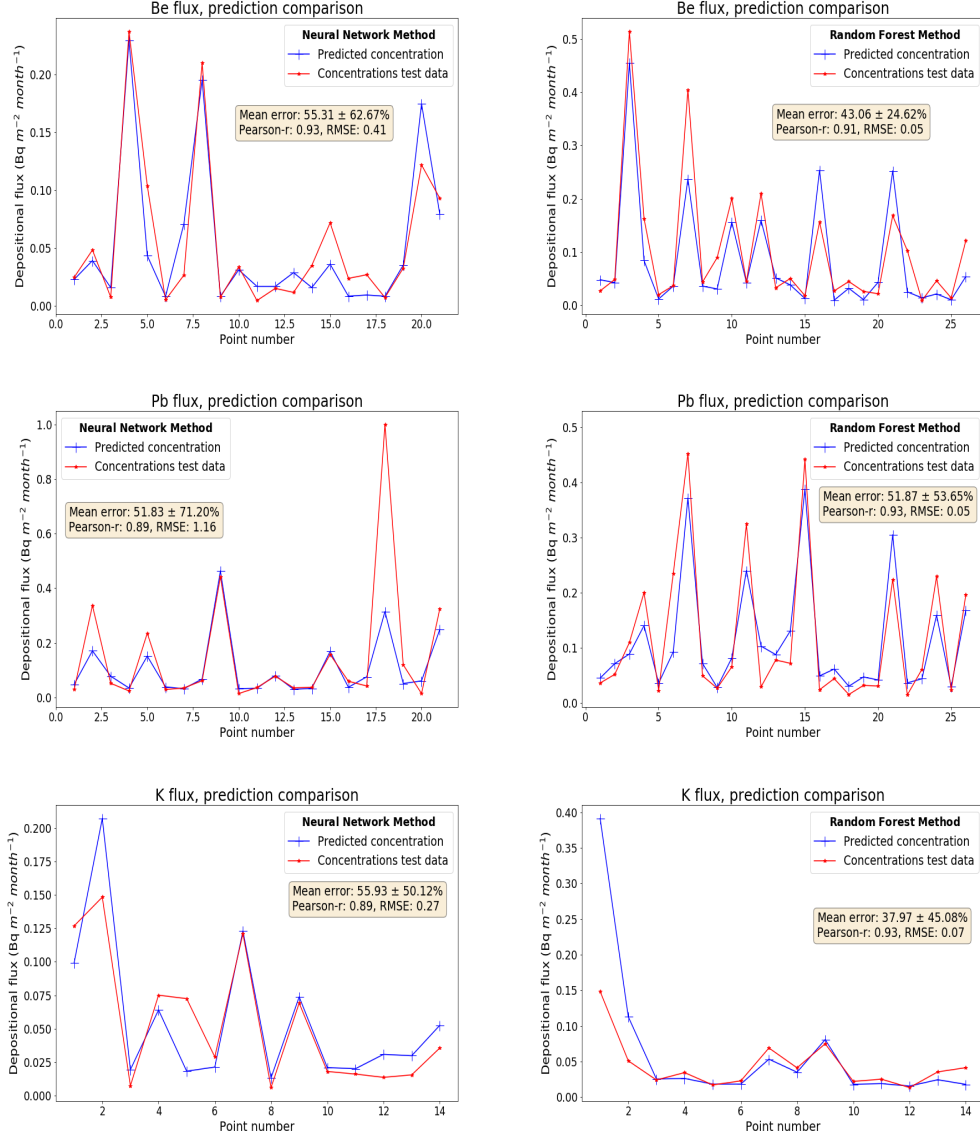


**Figure 2.** Example of the results of the predictions found from the Neural Network (left panels) and Random Forest (right panels) models. These predictions are limited to the test sample, which is chosen to be around a 20% of the full data set. We also include the values of the metrics used to evaluate the predictive ability of these methods, which are the Pearson-R correlation coefficient and the mean absolute error and its standard deviation. The root mean square error (RMSE), in units of  $Bq\ m^{-2}\ month^{-1}$ , is also included for completeness.

282 dian values and mode values more deviated from 0, but no significant differences between  
 283 same algorithms for different nuclides was detected.

284 Nevertheless, the evaluation of the models is highly dependent on the data set used.  
 285 From one side, the larger the test set, the more reliable is the model performance eval-  
 286 uation, but at the cost of reducing the number of samples used in the training set. On  
 287 the other side, if the test set is too short, the model performance evaluation will be very  
 288 uncertain. In this case, we observed that using around 20% of the full data set allowed

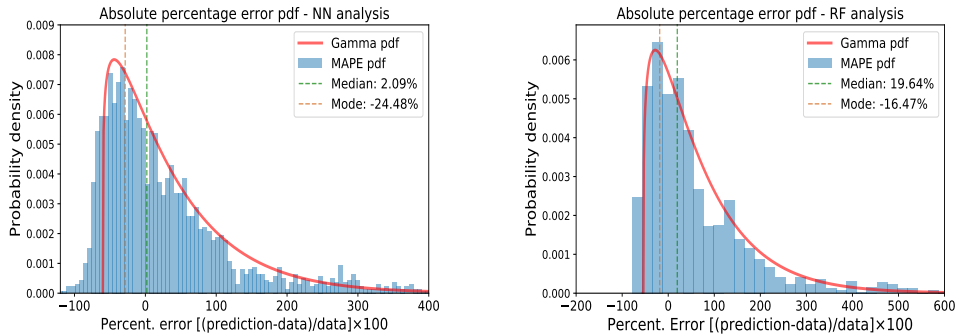


**Figure 3.** Probability distribution for the percentage errors found for various evaluations with (around 20) different tests sets. The left plot shows the results of these evaluations for the Neural Network algorithm and the right plot those for the Random Forest algorithm.

289 us to make consistent evaluations. Even though, they are still short enough to make our  
 290 evaluation very dependent on the data test used. This issue is well known by the ML  
 291 community and there are many possible strategies to deal with it to have an unbiased  
 292 evaluation of our model (Raschka, 2018) and its predictions uncertainties, as it is explored  
 293 in the next section.

#### 294 4.1 Statistical evaluation

295 To prevent from biasing our model evaluation by the small amount of test data used  
 296 and have into account the full uncertainty involved, we evaluate the algorithms by means  
 297 of a k-fold procedure. In this process the data set is divided into k subsets. Each time,  
 298 one of the k subsets is used as test set and the other k-1 subsets form the training set.  
 299 Then, we statistically combine the results to get solid conclusions.

300 At this point, another difference between the Neural Network and the Random For-  
 301 est algorithms should be taken into account to correctly manage the full uncertainties  
 302 involved: while the training process exactly results in the same model for the Random  
 303 Forest algorithm, this is subject to further fluctuations in the Neural Network algorithm.  
 304 This is due to the optimization procedure necessary for finding the minimum error or  
 305 loss when evaluating the examples in the training dataset. The main problems usually  
 306 faced are: getting stacked in local minimal or local optima (i.e. regions where the loss  
 307 is relatively low but it is not the lowest), saddle or flat points (regions where adjustments  
 308 of the training weights do not lead to an appreciable change in the loss) and other is-  
 309 sues more related with the loss function, gradients and the dimensionality involved. More  
 310 precise information about these problems can be found, e.g., in ref. Bengio (2012). There-  
 311 fore, each time the Neural Network is trained, specially when the number of samples is  
 312 not large enough, it is subject to small variations in the model predictions. For this rea-  
 313 son, a good evaluation of the uncertainties involved in the predictions of the Neural Net-  
 314 work model requires to add these fluctuations.

315 In particular, we repeated the training and test phase for 5 times with the same  
 316 test and training datasets. Then, we perform the evaluations with 20 different randomly-  
 317 selected test sub-datasets following the k-fold procedure. This means that we carry out  
 318 a total of 100 training and evaluation steps to determine the Pearson-R value and the  
 319 mean percentage error of our predictions with respect to the experimental data, as well  
 320 as the uncertainties related to these determinations for the Neural Network model. In  
 321 turn, as the Random Forest algorithm does not suffer from those training fluctuations,

322 we performed 60 evaluations of the model, employing a different test and training sub-  
 323 sets, accordingly, in each evaluation.

324 These results are shown in Figure 4, where we represent the mean Pearson-R in-  
 325 dex values and the  $1\sigma$  uncertainty related to its determination for both, the Neural Net-  
 326 works and Random Forest algorithms and for the three nuclides with respect to the num-  
 327 ber of iterations employed in the training phase. In general, we observe that the mean  
 328 Pearson-R index values are larger for the  $^7\text{Be}$  and  $^{210}\text{Pb}$  radionuclides, while  $^{40}\text{K}$  shows  
 329 the opposite, due to the smaller number of samples available. In addition, the uncertain-  
 330 ties related to the determination of the R index value from the Random Forest algorithm  
 331 is slightly larger than that from the NN algorithm. The mean Pearson-R index values  
 332 obtained are between 0.75-0.88 for  $^7\text{Be}$  and  $^{210}\text{Pb}$ , but around 0.7-0.8 for  $^{40}\text{K}$ , although  
 333 the errors are still high for every radionuclide. In particular, the determination of  $^7\text{Be}$   
 334 seems to be the most accurate in general, showing a  $1\sigma$  uncertainty in the determina-  
 335 tion of the R index value around  $\pm 0.065$  for the NN algorithm and  $\pm 0.08$  for the RF al-  
 336 gorithm. A maximum mean R index value of around 0.87 and 0.88 are found for  $^7\text{Be}$  and  
 337  $^{210}\text{Pb}$ , respectively, at 1400 and 1300 iterations. The maximum mean R index value ob-  
 338 tained for  $^{40}\text{K}$  is slightly above 0.8, found with the RF algorithm.

339 As expected, the performance of these methods in reproducing depositional fluxes  
 340 improves when having more samples, obtaining larger Pearson-R index values and lower  
 341 uncertainties related. Nevertheless, we observed that the NN algorithm seems to accuse  
 342 more the smaller number of samples with respect to the RF technique.

## 343 4.2 Selecting the main variables

344 To fully exploit the capability of ML techniques in improving our predictions in the  
 345 depositional fluxes, we determined which are the most important features using the re-  
 346 cursive feature elimination algorithm (RFE), which allows us to reduce the complexity  
 347 and needed cpu time of the Neural Network and Random Forest algorithms and prevents  
 348 from over-fitting our results. In addition, we compared the results obtained with these  
 349 features with those obtained when using all the features. Specifically, we used the *RFECV*  
 350 method from the *sklearn.feature\_selection* python package. The RFE algorithm is a fea-  
 351 ture selection method that allows a model to progressively eliminate the weakest features  
 352 and find the best scoring combination of features.

353 In Figure 5 we show the optimal important features found by the RFE algorithm,  
 354 along with their relative importance. As expected, the rainfall duration and rainfall vol-  
 355 ume are selected by the three radionuclides. Then, we observe that other atmospheric  
 356 variables are present, as the number of humid or dry days, the average monthly pres-  
 357 sure or the mean air temperature. On the other hand, the PM10 level and sunspot num-  
 358 ber are selected as important for the  $^{40}\text{K}$  nuclide.

359 The fact that the sunspot number arises as one of the most important variables de-  
 360 scribing the depositional fluxes of  $^{210}\text{Pb}$  and  $^{40}\text{K}$  is unexpected. In principle, this vari-  
 361 able is expected to be relevant for the production of  $^7\text{Be}$  since it is related with the so-  
 362 lar activity (this is, the Sun's magnetic field), which plays an important role on the flux  
 363 of cosmic rays reaching the atmosphere (Yoshimori et al., 2003). This fact is probably  
 364 due to the mild correlations between sunspot number and other atmospheric variables,  
 365 but more data samples are needed to get a solid conclusion, since the sunspot number  
 366 follows cycles of 11 and 22 years, following the solar magnetic cycles (E.W., 2015). This  
 367 could be explained by the fact that there are other correlations found between the so-  
 368 lar cycle and other atmospheric variables, as the atmospheric temperature (Qu et al.,  
 369 2012) and correlations with the cosmic-ray intensity at Earth, which is known to be re-  
 370 lated to climate and involved in processes of cloud formation (Veretenenko et al., 2018;  
 371 Svensmark et al., 2013; Marsh & Svensmark, 2000).

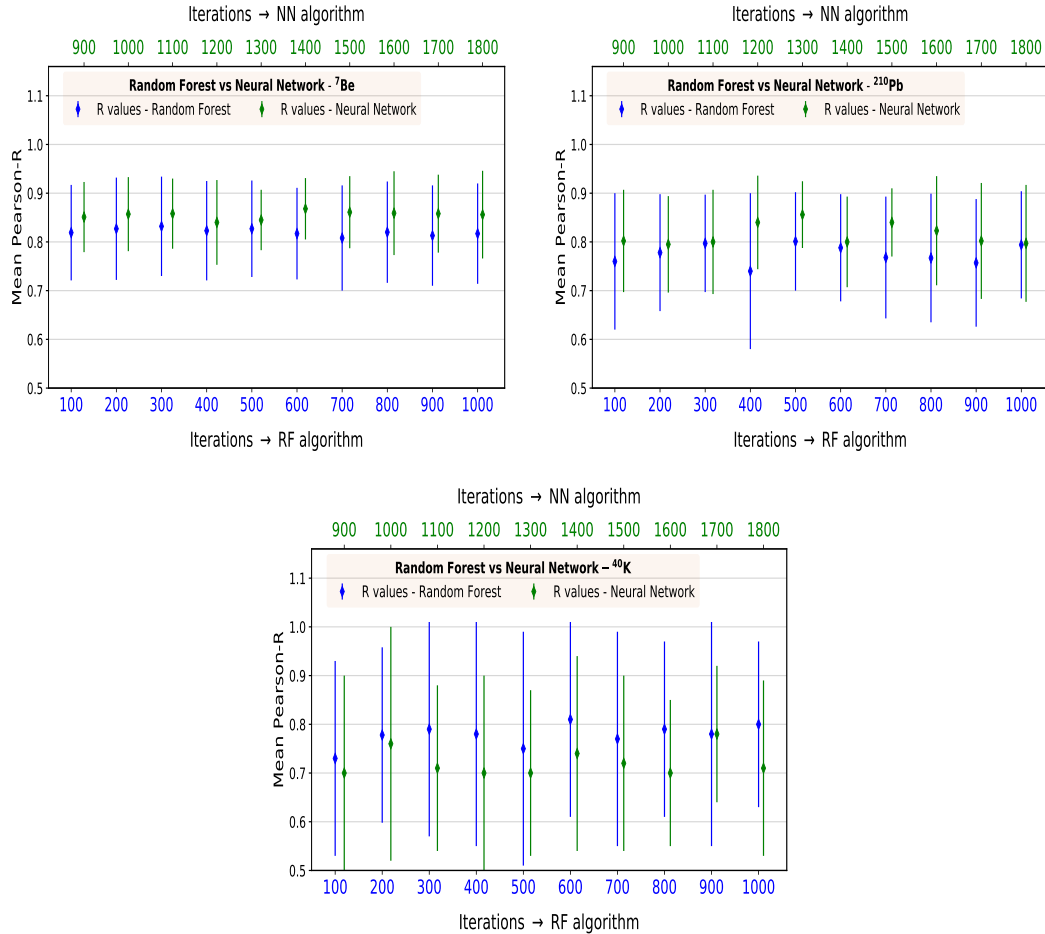


**Figure 4.** Results from the  $k$ -fold evaluation of the Pearson- $R$  correlation coefficient for the Neural Network and Random Forest algorithms for the depositional fluxes of  ${}^7\text{Be}$  (upper panel),  ${}^{210}\text{Pb}$  (middle panel) and  ${}^{40}\text{K}$  (lower panel). The results obtained from the NN algorithm are shown in green while the results from the RF algorithm are shown in blue.

372 Once these features have been selected, we proceed to compare the NN and RF al-  
 373 gorithms explored in this work using all the features and using just the important fea-  
 374 tures, as displayed in Figure 6. From this figure, we can see that the NN models for  ${}^{40}\text{K}$   
 375 have significantly improved, restricting our features to be just the important ones. This  
 376 means that some of the eliminated features were over-fitting the model. This can be re-  
 377 lated to the fact that this radionuclide actually comes from African zones and reach coastal  
 378 zones of Southern Spain after it is transported by winds in the correct direction. There-  
 379 fore, some of the atmospheric variables measured in the zone of Malaga could not be suit-  
 380 able to describe its amount and depositions in Malaga. Even though, the amount of rain-  
 381 fall should still be crucial to make the African dust to definitely fall in the study region.  
 382 Furthermore, the presence of the sunspot number as an important feature have not been  
 383 pointed out in the past, which may mean that there are other atmospheric variables with  
 384 a considerable role in the amount and depositional flux of  ${}^{40}\text{K}$  found in the Mediterranean  
 385 coastal zone of the Southern Spain.

386 On the other hand, we see that for  ${}^7\text{Be}$  and  ${}^{210}\text{Pb}$  the results remain very similar  
 387 to the case with all the features, which is quite remarkable given the number of variables

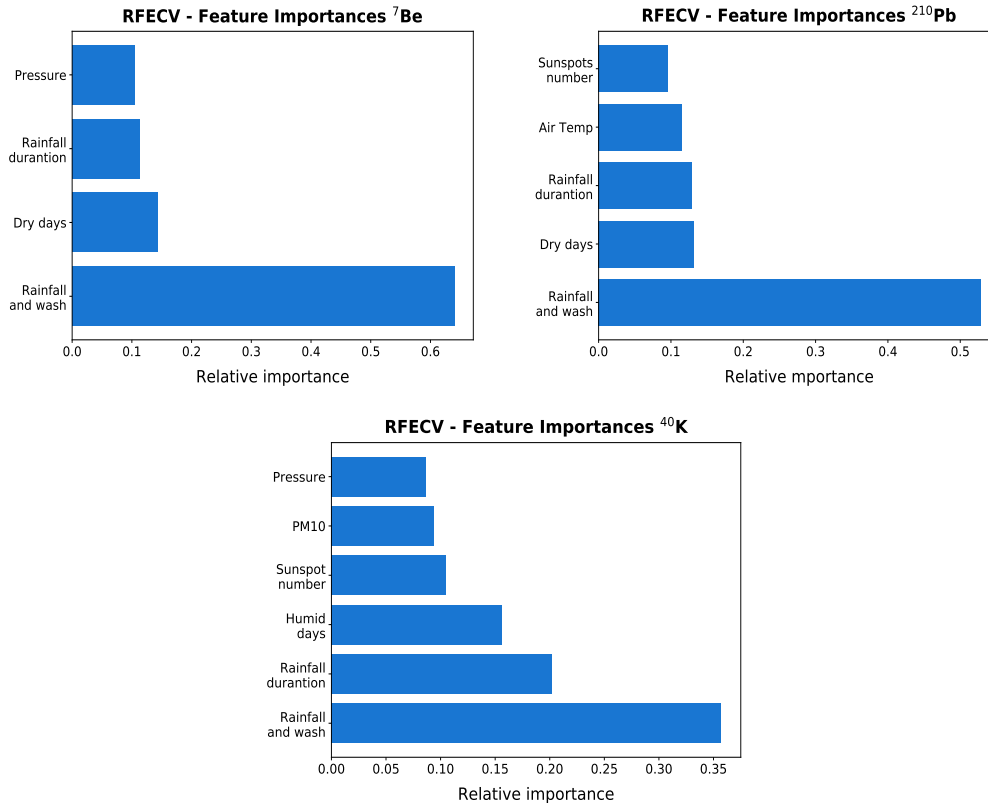


**Figure 5.** Histograms with the important features found with the implemented recursive feature elimination algorithm for the depositional fluxes of  $^7\text{Be}$  (upper panel),  $^{210}\text{Pb}$  (middle panel) and  $^{40}\text{K}$  (lower panel) with their relative importance.

388 needed. In addition, the uncertainties related to the determination of the Pearson-R cor-  
 389 relation coefficient have been considerably reduced in the NN models for  $^{40}\text{K}$ , while they  
 390 seem to be almost identical for all other cases.

391 In general, these results are consistent with other previously found, but the use of  
 392 these ML methods allow our predictions to be more complex and better adapt to the vari-  
 393 ability related to the depositional fluxes of different radionuclides.

## 394 5 Conclusions

395 Modern computer algorithms allow us to refine our measurements and model pre-  
 396 dictions via new statistical tools or artificial intelligence. In this work, we have made use  
 397 of two common machine learning algorithms, Neural Networks and Random Forests, in  
 398 order to predict and analyse the depositional fluxes of  $^7\text{Be}$  and  $^{210}\text{Pb}$  and  $^{40}\text{K}$ . This work  
 399 has shown, first, that these methods can be successfully applied to study the depositional  
 400 fluxes of different radionuclides from atmospheric variables as the amount of rainfall, pres-  
 401 sure or air temperatures. Second, we have evaluated the performance of these models  
 402 using a k-fold method and the Pearson-R coefficient and mean absolute error as metrics  
 403 finding that these techniques can significantly improve old predictions made from mul-  
 404 tivariate linear regression analyses.

405 As expected, the performance of these methods in reproducing depositional fluxes  
 406 improves when having more samples, obtaining larger Pearson-R index values and lower

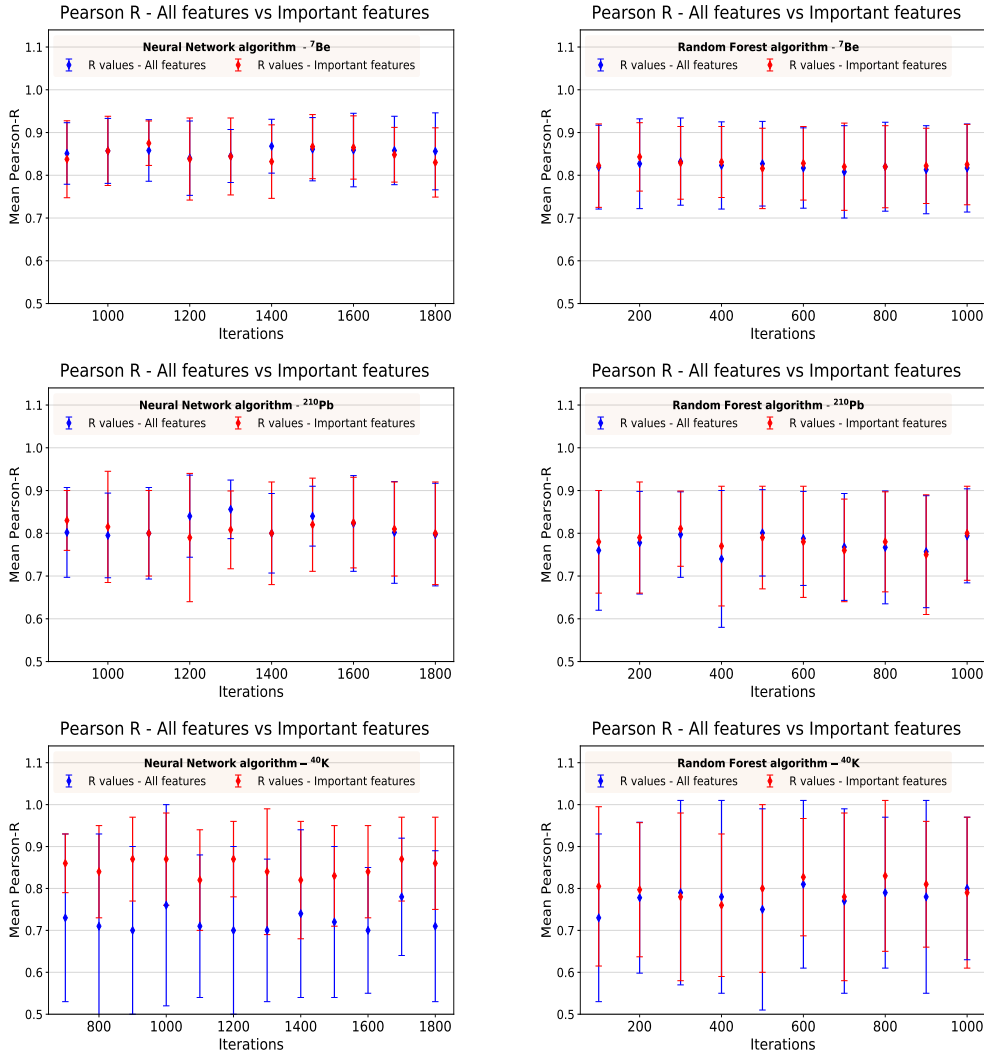


**Figure 6.** Same as in Figure 4, but comparing now the results obtained using the main variables obtained from the RFE algorithm and those obtained from the models trained with all the available variables in the data set.

407 uncertainties related. This, in fact, confirms the prospects on future models, with a larger  
 408 number of samples measured. This is mainly related to the long times involved in the  
 409 natural cycles of atmospheric variables, as, for example, the sunspot number, which is  
 410 known to follow 11 or 22-years periods (solar magnetic cycles). Nonetheless, we have demon-  
 411 strated that the algorithms employed here are able to reproduce the experimental depo-  
 412 sitional fluxes using monthly-averaged variables and that these predictions can help  
 413 identifying periods of anomalous radiation doses. Interestingly, we found that both, the  
 414 depositional fluxes of  $^{210}\text{Pb}$  and  $^{40}\text{K}$ , seem to be correlated with the Sunspot number.

415 The Neural Network models seem to reach higher mean Pearson-R index values,  
 416 calculated using a k-fold cross-validation treatment, almost reaching 0.9, although the  
 417 uncertainties are still quite high. Furthermore, the use of a Recursive Feature Elimina-  
 418 tion algorithm has been used to find the variables that perform the best predictions and  
 419 allow us to reduce to 4, 5 and 6 the number of variables used for predicting the depo-  
 420 sitional fluxes of  $^7\text{Be}$ ,  $^{210}\text{Pb}$  and  $^{40}\text{K}$ , respectively. The training of the Neural Network

421 and Random Forest models with these variables resulted into a negligible difference in  
 422 the Pearson-R index values and the uncertainties related to its determination except for  
 423 the  $^{40}\text{K}$  nuclide in the Neural Network model, which showed a significant improvement.  
 424 Even with this reduced number of variables used for training our methods, we were able  
 425 to obtain mean values for the Pearson-R index value above 0.80 for all the three nuclides  
 426 and both algorithms. A maximum mean R index value around 0.87 is found for  $^7\text{Be}$ ,  $^{210}\text{Pb}$   
 427 and  $^{40}\text{K}$ , respectively, at 1400, 1300 and 1200 iterations for the Neural Network method.  
 428 For the Random Forest method, the maximum mean R index value of *sim*0.81 is found  
 429 around 500 and 600 iterations for  $^{210}\text{Pb}$  and  $^{40}\text{K}$  and of almost 0.85 for the  $^7\text{Be}$  radionu-  
 430 clide.

431 In conclusion, we demonstrate that Random Forest and Neural Networks methods  
 432 are able to improve our current knowledge and predictions on the depositional fluxes of  
 433 radionuclides in the Mediterranean coastal zone of Malaga and these models can be ex-  
 434 tended to other zones too, in order to build a more complex ensemble that could refine  
 435 the existent knowledge on deposition of different radionuclides. Thus, this work consti-  
 436 tutes the first step into the study of a large-scale (in terms of geographical areas) model  
 437 able to make predictions on depositional fluxes for different geographical zones thanks  
 438 to the adaptability of these algorithms. The implementation of a recurrent neural net-  
 439 work applied to the prediction of depositional fluxes can improve these models and will  
 440 be also investigated in a next work.

#### 441 Acknowledgments

442 We would like to express our gratitude to the Consejo de Seguridad Nuclear, Spain,  
 443 for their financial support to the Environmental Radioactivity Laboratory of the Uni-  
 444 versity of Málaga.

#### 445 References

- 446 Baskaran, M., Coleman, C. H., & Santschi, P. H. (1993). Atmospheric depositional  
 447 fluxes of  $^7\text{be}$  and  $^{210}\text{pb}$  at galveston and college station, texas. *Journal of*  
 448 *Geophysical Research: Atmospheres*, 98(D11), 20555-20571. Retrieved from  
 449 <https://agupubs.onlinelibrary.wiley.com/doi/abs/10.1029/93JD02182>  
 450 doi: <https://doi.org/10.1029/93JD02182>
- 451 Bengio, Y. (2012). Practical recommendations for gradient-based training of deep  
 452 architectures. In G. Montavon, G. B. Orr, & K. Müller (Eds.), *Neural net-*  
 453 *works: Tricks of the trade - second edition* (Vol. 7700, pp. 437-478). Springer.  
 454 Retrieved from [https://doi.org/10.1007/978-3-642-35289-8\\_26](https://doi.org/10.1007/978-3-642-35289-8_26) doi:  
 455 10.1007/978-3-642-35289-8\_26
- 456 Bergstra, J., & Bengio, Y. (2012, February). Random search for hyper-parameter  
 457 optimization. *J. Mach. Learn. Res.*, 13(null), 281-305.
- 458 Carbonell, J. G., Michalski, R. S., & Mitchell, T. M. (1983). Machine learning: a  
 459 historical and methodological analysis. *AI Magazine*, 4(3), 69-69.
- 460 Chham, E., Piñero-García, F., Brattich, E., El Bardouni, T., & Ferro-García, M.  
 461 (2018).  $^7\text{be}$  spatial and temporal pattern in southwest of europe (spain): Eval-  
 462 uation of a predictive model. *Chemosphere*, 205, 194 - 202. Retrieved from  
 463 <http://www.sciencedirect.com/science/article/pii/S0045653518307483>  
 464 doi: <https://doi.org/10.1016/j.chemosphere.2018.04.099>
- 465 Chollet, F. (2015). *Keras*. <https://github.com/fchollet/keras>. GitHub.
- 466 Dueñas, C., Fernández, M., Carretero, J., Liger, E., & Cañete, S. (2004). Long-  
 467 term variation of the concentrations of long-lived rn descendants and cosmo-  
 468 genic  $^7\text{be}$  and determination of the mrt of aerosols. *Atmospheric Environ-*  
 469 *ment*, 38(9), 1291 - 1301. Retrieved from [http://www.sciencedirect.com/](http://www.sciencedirect.com/science/article/pii/S1352231003010549)  
 470 [science/article/pii/S1352231003010549](http://www.sciencedirect.com/science/article/pii/S1352231003010549) doi: <https://doi.org/10.1016/>

- 471 j.atmosenv.2003.11.029
- 472 Dueñas, C., Fernández, M., Cañete, S., & Pérez, M. (2009). 7be to 210pb con-  
 473 centration ratio in ground level air in Málaga (36.7°N, 4.5°W). *Atmospheric*  
 474 *Research*, 92(1), 49 - 57. Retrieved from [http://www.sciencedirect.com/](http://www.sciencedirect.com/science/article/pii/S0169809508002342)  
 475 [science/article/pii/S0169809508002342](http://www.sciencedirect.com/science/article/pii/S0169809508002342) doi: [https://doi.org/10.1016/](https://doi.org/10.1016/j.atmosres.2008.08.012)  
 476 [j.atmosres.2008.08.012](https://doi.org/10.1016/j.atmosres.2008.08.012)
- 477 Dueñas, C., Fernández, M., Gordo, E., Cañete, S., & Pérez, M. (2011). Gross  
 478 alpha, gross beta activities and gamma emitting radionuclides composition  
 479 of rainwater samples and deposition to ground. *Atmospheric Environment*,  
 480 45(4), 1015 - 1024. Retrieved from [http://www.sciencedirect.com/](http://www.sciencedirect.com/science/article/pii/S1352231010009313)  
 481 [science/article/pii/S1352231010009313](http://www.sciencedirect.com/science/article/pii/S1352231010009313) doi: [https://doi.org/10.1016/](https://doi.org/10.1016/j.atmosenv.2010.10.045)  
 482 [j.atmosenv.2010.10.045](https://doi.org/10.1016/j.atmosenv.2010.10.045)
- 483 Dueñas, C., Fernández, M., Gordo, E., Cañete, S., & Pérez, M. (2012). Chemical  
 484 and radioactive composition of bulk deposition in Málaga (Spain). *Atmospheric*  
 485 *Environment*, 62, 1-8. Retrieved from [https://www.sciencedirect.com/](https://www.sciencedirect.com/science/article/pii/S1352231012007595)  
 486 [science/article/pii/S1352231012007595](https://www.sciencedirect.com/science/article/pii/S1352231012007595) doi: [https://doi.org/10.1016/](https://doi.org/10.1016/j.atmosenv.2012.07.073)  
 487 [j.atmosenv.2012.07.073](https://doi.org/10.1016/j.atmosenv.2012.07.073)
- 488 Dueñas, C., Fernández, M., Liger, E., & Carretero, J. (1999). Gross alpha, gross  
 489 beta activities and 7be concentrations in surface air: analysis of their varia-  
 490 tions and prediction model. *Atmospheric Environment*, 33(22), 3705 - 3715.  
 491 Retrieved from [http://www.sciencedirect.com/science/article/pii/](http://www.sciencedirect.com/science/article/pii/S1352231099001727)  
 492 [S1352231099001727](http://www.sciencedirect.com/science/article/pii/S1352231099001727) doi: [https://doi.org/10.1016/S1352-2310\(99\)00172-7](https://doi.org/10.1016/S1352-2310(99)00172-7)
- 493 Dueñas, C., Gordo, E., Liger, E., Cabello, M., Ca, S., Pérez, M., & de la  
 494 Torre Luque, P. (2017, 11). 7 be, 210 pb and 40 k depositions over 11 years  
 495 in Málaga. *Journal of Environmental Radioactivity*, 178-179, 325-334. doi:  
 496 [10.1016/j.jenvrad.2017.09.010](https://doi.org/10.1016/j.jenvrad.2017.09.010)
- 497 Escudero, M., Castillo, S., Querol, X., Avila, A., Alarcón, M., Viana, M., ... Ro-  
 498 driguez, S. (2005, 09). Wet and dry African dust episodes over eastern Spain.  
 499 *Journal of Geophysical Research*, 110, 18-8. doi: [10.1029/2004JD004731](https://doi.org/10.1029/2004JD004731)
- 500 E.W., C. (2015). The extended cycle of solar activity and the sun's 22-year magnetic  
 501 cycle. *Space Sciences Series of ISSI*, 53. doi: [https://doi.org/10.1007/978-1-](https://doi.org/10.1007/978-1-4939-2584-1_6)  
 502 [4939-2584-1\\_6](https://doi.org/10.1007/978-1-4939-2584-1_6)
- 503 Garcia-Orellana, J., Sanchez-Cabeza, J. A., Masqué, P., Àvila, A., Costa, E., Lojè-  
 504 Pilot, M. D., & Bruach-Menchén, J. M. (2006). Atmospheric fluxes of 210pb  
 505 to the western Mediterranean sea and the Saharan dust influence. *Journal*  
 506 *of Geophysical Research: Atmospheres*, 111(D15). Retrieved from [https://](https://agupubs.onlinelibrary.wiley.com/doi/abs/10.1029/2005JD006660)  
 507 [agupubs.onlinelibrary.wiley.com/doi/abs/10.1029/2005JD006660](https://agupubs.onlinelibrary.wiley.com/doi/abs/10.1029/2005JD006660) doi:  
 508 <https://doi.org/10.1029/2005JD006660>
- 509 Graff, P., Feroz, F., Hobson, M. P., & Lasenby, A. (2014, 05). SkyNet: an ef-  
 510 ficient and robust neural network training tool for machine learning in as-  
 511 tronomy. *Monthly Notices of the Royal Astronomical Society*, 441(2), 1741-  
 512 1759. Retrieved from [https://doi.org/10.1093/mnras/](https://doi.org/10.1093/mnras/stu642)  
 513 [stu642](https://doi.org/10.1093/mnras/stu642) doi: [10.1093/mnras/stu642](https://doi.org/10.1093/mnras/stu642)
- 514 Herranz, M., Idoeta, R., & Legarda, F. (2008, 10). Evaluation of uncertainty and  
 515 detection limits in radioactivity measurements. *Nuclear Instruments and Meth-*  
 516 *ods in Physics Research Section A: Accelerators, Spectrometers, Detectors and*  
 517 *Associated Equipment*, 595, 526-534. doi: [10.1016/j.nima.2008.07.105](https://doi.org/10.1016/j.nima.2008.07.105)
- 518 Heydorn, K. (2004, 10). Evaluation of the uncertainty of environmental measure-  
 519 ments of radioactivity. *Journal of Radioanalytical and Nuclear Chemistry*, 262,  
 520 249-253. doi: [10.1023/B:JRNC.0000040882.22365.a7](https://doi.org/10.1023/B:JRNC.0000040882.22365.a7)
- 521 Karlsson, L., Hernandez, F., Rodriguez, S., Lopez-Perez, M., Hernandez-Armas, J.,  
 522 Alonso-Perez, S., & Cuevas, E. (2008). Using 137cs and 40k to identify natural  
 523 Saharan dust contributions to pm10 concentrations and air quality impairment  
 524 in the Canary Islands. *Atmospheric Environment*, 42(30), 7034-7042.
- 525 Lal, D., Malhotra, P. K., & Peters, B. (1958, January). On the production of ra-

- 526           dioxotopes in the atmosphere by cosmic radiation and their application to  
527           meteorology. *Journal of Atmospheric and Terrestrial Physics*, 12(4), 306-328.  
528           doi: 10.1016/0021-9169(58)90062-X
- 529   Lapedes, A., Barnes, C., Burks, C., Farber, R., & Sirotkin, K. (1988). *Application*  
530           *of neural networks and other machine learning algorithms to dna sequence*  
531           *analysis* (Tech. Rep.). Los Alamos National Lab., NM (USA).
- 532   Marsh, N., & Svensmark, H. (2000, 11). Cosmic rays, clouds, and climate. *Space Sci-*  
533           *ence Reviews*, 94, 215-230. doi: 10.1023/A:1026723423896
- 534   Martell, E. (1970). Transport patterns and residence times for atmospheric trace  
535           constituents vs. altitude. In (Vol. 93). ACS Publications. doi: 10.1021/ba-1970-  
536           -0093.ch009
- 537   Moore, H. E., Poet, S. E., & Martell, E. A. (1973). 222rn, 210pb, 210bi, and  
538           210po profiles and aerosol residence times versus altitude. *Journal of Geo-*  
539           *physical Research (1896-1977)*, 78(30), 7065-7075. Retrieved from [https://](https://agupubs.onlinelibrary.wiley.com/doi/abs/10.1029/JC078i030p07065)  
540           [agupubs.onlinelibrary.wiley.com/doi/abs/10.1029/JC078i030p07065](https://agupubs.onlinelibrary.wiley.com/doi/abs/10.1029/JC078i030p07065)  
541           doi: <https://doi.org/10.1029/JC078i030p07065>
- 542   Preiss, N., MéLièRes, M.-A., & Pourchet, M. (1996, December). A compilation  
543           of data on lead 210 concentration in surface air and fluxes at the air-surface  
544           and water-sediment interfaces. *Journal of Geophysical Research*, 101(D22),  
545           28,847-28,862. doi: 10.1029/96JD01836
- 546   Qu, W., Zhao, J., Huang, F., & Deng, S. (2012, jun). CORRELATION BETWEEN  
547           THE 22-YEAR SOLAR MAGNETIC CYCLE AND THE 22-YEAR QUA-  
548           SICYCLE IN THE EARTH'S ATMOSPHERIC TEMPERATURE. *The*  
549           *Astronomical Journal*, 144(1), 6. Retrieved from [https://doi.org/10.1088/](https://doi.org/10.1088/0004-6256/144/1/6)  
550           [0004-6256/144/1/6](https://doi.org/10.1088/0004-6256/144/1/6) doi: 10.1088/0004-6256/144/1/6
- 551   Raschka, S. (2018, 11). Model evaluation, model selection, and algorithm selection in  
552           machine learning. *ArXiv preprint <https://arxiv.org/abs/1811.12808v3>*.  
553           Retrieved from <https://arxiv.org/abs/1811.12808v3>
- 554   Sarkar, K., Ghalia, M. B., Wu, Z., & Bose, S. C. (2009). A neural network model  
555           for the numerical prediction of the diameter of electro-spun polyethylene oxide  
556           nanofibers. *Journal of Materials Processing Technology*, 209(7), 3156 - 3165.  
557           Retrieved from [http://www.sciencedirect.com/science/article/pii/](http://www.sciencedirect.com/science/article/pii/S0924013608005827)  
558           [S0924013608005827](http://www.sciencedirect.com/science/article/pii/S0924013608005827) doi: <https://doi.org/10.1016/j.jmatprotec.2008.07.032>
- 559   Schaefer, C., Geiger, M., Kuntzer, T., & Kneib, J.-P. (2018). Deep convolutional  
560           neural networks as strong gravitational lens detectors. *A&A*, 611, A2. Re-  
561           trieved from <https://doi.org/10.1051/0004-6361/201731201> doi: 10.1051/  
562           0004-6361/201731201
- 563   Schuler, C., Wieland, E., Santschi, P. H., Sturm, M., Lueck, A., Bollhalder, S.,  
564           ... Wolffi, W. (1991). A multitracer study of radionuclides in lake zurich,  
565           switzerland: 1. comparison of atmospheric and sedimentary fluxes of 7be, 10be,  
566           210pb, 210po, and 137cs. *Journal of Geophysical Research: Oceans*, 96(C9),  
567           17051-17065. Retrieved from [https://agupubs.onlinelibrary.wiley.com/](https://agupubs.onlinelibrary.wiley.com/doi/abs/10.1029/91JC01765)  
568           [doi/abs/10.1029/91JC01765](https://agupubs.onlinelibrary.wiley.com/doi/abs/10.1029/91JC01765) doi: <https://doi.org/10.1029/91JC01765>
- 569   Svensmark, H., Enghoff, M. B., & Pedersen, J. O. P. (2013). Response of cloud  
570           condensation nuclei (>50 nm) to changes in ion-nucleation. *Physics Letters*  
571           *A*, 377(37), 2343 - 2347. Retrieved from [http://www.sciencedirect.com/](http://www.sciencedirect.com/science/article/pii/S0375960113006294)  
572           [science/article/pii/S0375960113006294](http://www.sciencedirect.com/science/article/pii/S0375960113006294) doi: [https://doi.org/10.1016/](https://doi.org/10.1016/j.physleta.2013.07.004)  
573           [j.physleta.2013.07.004](https://doi.org/10.1016/j.physleta.2013.07.004)
- 574   Veretenenko, S., Ogurtsov, M., Lindholm, M., & Jalkanen, R. (2018). Galac-  
575           tic cosmic rays and low clouds: Possible reasons for correlation rever-  
576           sal. In Z. Szadkowski (Ed.), *Cosmic rays* (chap. 5). Rijeka: IntechOpen.  
577           Retrieved from <https://doi.org/10.5772/intechopen.75428> doi:  
578           10.5772/intechopen.75428
- 579   vStencl, M., & Stastny, J. (2011, 04). Artificial neural networks numerical forecast-  
580           ing of economic time series. In (p. 15+). IntechOpen.

- 581 Wilkening, M., Clements, W., & Stanley, D. (1975). Radon 222 flux measurements  
582 in widely separated regions. *Natural radiation environment II*, 717-730.
- 583 Williams, N., Zander, S., & Armitage, G. (2006, October). A preliminary per-  
584 formance comparison of five machine learning algorithms for practical ip  
585 traffic flow classification. *SIGCOMM Comput. Commun. Rev.*, 36(5),  
586 5–16. Retrieved from <https://doi.org/10.1145/1163593.1163596> doi:  
587 10.1145/1163593.1163596
- 588 Wogman, N. A., Thomas, C. W., Cooper, J. A., Engelmann, R. J., & Perkins,  
589 R. W. (1968). Cosmic ray-produced radionuclides as tracers of atmo-  
590 spheric precipitation processes. *Science*, 159(3811), 189–192. Retrieved  
591 from <https://science.sciencemag.org/content/159/3811/189> doi:  
592 10.1126/science.159.3811.189
- 593 Yoshimori, M., Hirayama, H., Mori, S., Sasaki, K., & Sakurai, H. (2003). Be-7 nuclei  
594 produced by galactic cosmic rays and solar energetic particles in the earth's  
595 atmosphere. *Advances in Space Research*, 32(12), 2691 - 2696. Retrieved from  
596 <http://www.sciencedirect.com/science/article/pii/S0273117703800856>  
597 doi: <https://doi.org/10.1016/j.asr.2003.07.006>

598  
599**Appendix A Sketches of Neural Network and Random Forest structures**600  
601  
602

In this appendix, we show a sketch of the general structure of the Neural Network model employed and an example of a branch of a decision tree from the Random Forest algorithm investigated in this work.

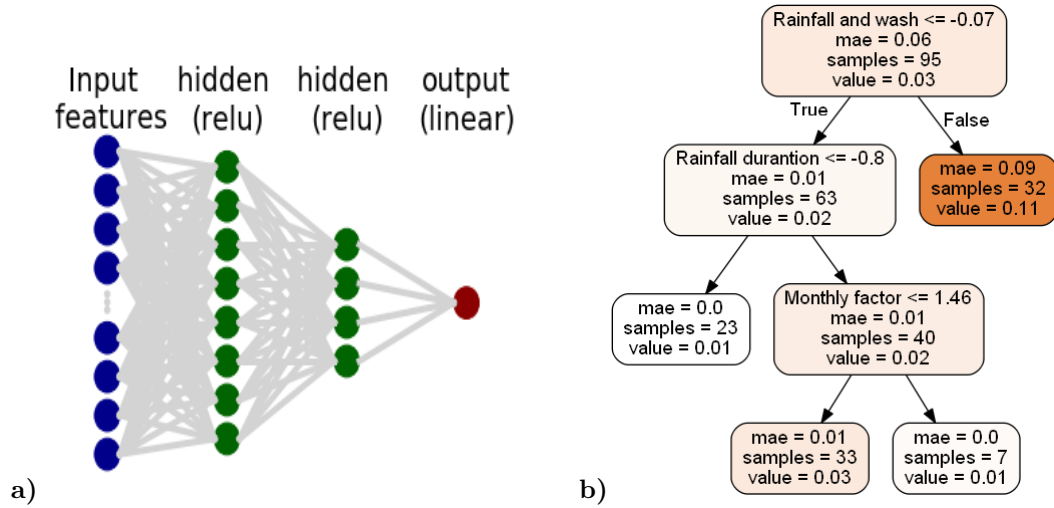


**Figure A1.** a): Sketch of the Neural Network model used, where there are two hidden layers that use the ReLU activation function and an output unit that linearly combines the nodes of the last hidden layer. b): Example of a decision tree used as part of a Random Forest model.

603 **Appendix B Sketches of Neural Network and Random Forest struc-**  
 604 **tures**

605 This appendix shows a comparison between the predictions from the reference model  
 606 and the depositional flux measurements for one of these samples. It is crucial to have  
 607 a reference model evaluated in the same way as for the ML algorithms studied in the pa-  
 608 per, since this kind of evaluation is rather peculiar from ML algorithms. As we see, tra-  
 609 ditional models, based in linear regressions, are unable to reproduce the depositional fluxes  
 610 behaviour, because of the complex relationships between variables.

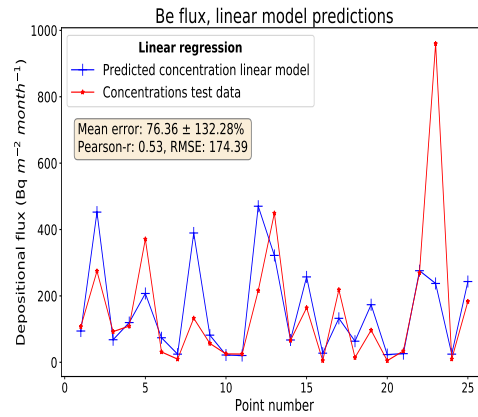


**Figure B1.** Predictions found from the reference linear model on one of the 25-length data samples, using the same evaluation as for the Random Forest and Neural Network algorithms studied in this work. Units of RMSE are of  $Bq\ m^{-2}\ month^{-1}$ .